High contrast ratio prism design in a mini projector

Jui-Wen Pan[1,2,3,*] and Hsiang-Hua Wang[4]

[1]Institute of Photonic System, National Chiao Tung University, Tainan City 71150, Taiwan

[2]Biomedical Electronics Translational Research Center, National Chiao Tung University, Hsin-Chu City 30010, Taiwan

[3]Department of Medical Research, Chi Mei Medical Center, Tainan 71004, Taiwan

[4]Institute of Imaging and Biomedical Photonics, National Chiao Tung University, Tainan City 71150, Taiwan

*Corresponding author: juiwenpan@gmail.com

Received 22 August 2013; revised 29 October 2013; accepted 29 October 2013;
posted 30 October 2013 (Doc. ID 196241); published 25 November 2013

In this paper, we present a novel prism with the ability to enhance the contrast ratio and maintain the optical efficiency in a digital light processing projection system. The working theorem for the novel prism is derived as well. In this novel prism design, the ghost ray is directed away from the projection lens by a total internal reflection surface. Since the ghost ray does not even enter the projection lens, the contrast ratio enhancement is more effective than that achieved by an asymmetrical stop. Compared with the conventional method, the full-on/full-off contrast ratio is increased from 921:1 to 46347:1 and the American National Standards Institute contrast ratio is increased from 177:1 to 295:1. The imaging system efficiency can maintain at 79.8% under the contrast ratio enhancement process. Ghost ray analysis for the novel prism explains the contrast enhancement well.

OCIS codes: (230.3670) Light-emitting diodes; (230.5480) Prisms; (330.1800) Vision - contrast sensitivity; (110.2945) Illumination design.

http://dx.doi.org/10.1364/AO.52.008347

1. Introduction

Personal displays are widely recognized as necessary to today's lifestyles, especially in mobile phones, which are used for communication and data sharing. However, the goal of making a projector that can be embedded into a mobile phone remains out of reach. In this respect, the light-emitting diode (LED) projector [1,2] has attracted much attention in recent years due to its portability. Image information could be shared much more easily by using such a small and lightweight device. The possibility of embedding an LED-projector in other media devices such as a mobile phone or notebook makes their development more attractive and more promising at the present time [2–4]. The recent growth in popularity of the smartphone has sped up LED-projector development. Digital light processing (DLP) [5,6] projection systems, based on the Texas Instruments Digital Micromirror Device (DMD) [7], are one of the main technologies that dominate the projector market now. The DLP projection system obtains higher efficiency and a better contrast ratio by avoiding the use of polarization optics. Also, the maturity of the manufacturing techniques makes it superior to other projection systems.

DLP-projector technology has demonstrated great improvement in the last few years. The optical efficiency and system volume of DLP projectors have been improved. However, the DLP projector's image quality still cannot compare with that of other display systems. In the projector manufacturing industry, the contrast ratio is an important feature of image quality. The contrast ratio is mainly affected by the quantity of uncontrolled light (which is produced by scattered light and using a nonideal coating) entering the projection lens. In order to collect more light in the pupil of the projection lens for higher efficiency, a smaller f-number projection

1559-128X/13/348347-08$15.00/0

system is usually used in a DLP projection system [8]. However, this method also causes more uncontrolled light to enter the projection lens. To enhance the contrast ratio and maintain the efficiency of the LED projector, the problem of uncontrolled light related to the use of a smaller f-number projection system needs to be dealt with.

One common way to increase the contrast ratio of the DLP projector and maintain the optical efficiency is the addition of an asymmetric stop in the projection lens [8,9]. The asymmetric stop blocks flat-state light and uncontrolled light from passing through the projection lens stop. Although this method can really improve the projector's contrast ratio and maintain optical efficiency [8], it still has some disadvantages that need to be improved. The main disadvantage is the lens alignment with the asymmetric stop. There is a relationship between the orientation of the asymmetric stop and the angle of rotation of the micromirrors [10,11]. The orientation of the asymmetric stop increases the manufacturing difficulty for lens alignment. Moreover, the uncontrolled light blocked by the asymmetric stop in the projection lens can still affect the contrast ratio by becoming an extra source of scattered light in the projection lens. The extra scattered light might still strike the screen after being reflected many times within the projection lens. In a word, it is hard to reach a really high contrast ratio with the asymmetric stop method.

In this paper, we propose a novel prism designed to enhance the contrast ratio and maintain the optical efficiency in a DLP projection system. The novel prism has the ability to reflect the uncontrolled light away from the projection lens without any additional asymmetric stop. The contrast ratio can be effectively enhanced, and the disadvantage of the traditional asymmetric stop method, which affects lens alignment, can be improved. The novel prism can be easily designed using the derived mathematical equations. Optical software is used to simulate the imaging system and analyze the efficiency and contrast ratio. In order to find the reason for the contrast enhancement, ghost analysis of the optical ray path is carried out. The traditional asymmetric stop method lets flat-state light into the projection lens, inducing some light scattering, which affects the contrast ratio. This phenomenon is reduced with the novel prism.

2. Working Principles of the Novel Prism

The DLP projectors can be grouped into two types, depending on the architecture: the telecentric architecture or nontelecentric architecture. In the telecentric architecture, a prism is used to avoid interference between the illumination ray path and the image ray path in the projection system [6]. Compared with the nontelecentric architecture, the telecentric architecture DLP projector has higher uniformity owing to the telecentric condition at the DMD's active area [12]. The illumination system and projection system of the telecentric architecture can be designed independently [6]. This feature makes the design easier. Therefore, the telecentric architecture has become the most commonly used design in the DLP projection system [2,8,13,14].

For display applications, the contrast is the most important factor. In the telecentric architecture, the prism is one of the main factors affecting the contrast ratio. Removing flat-state light scattering is the main issue in contrast enhancement. Figure 1 shows a schematic diagram of the novel prism. The prism is composed of three prisms of the same material. There are air gaps between the different prisms. To prevent astigmatism, the air gaps are usually less than 10 μm [6]. Given the limitations of the manufacturing technology, the air gaps are usually controlled at 5 μm [15,16]. The direction of the ray path changes due to total internal reflection (TIR) at the air gaps. In this design, the two air gaps of the novel prism are defined as the first TIR surface (orange line) and the second TIR surface (red line). When the light strikes the two TIR surfaces, TIR occurs when the incident angle is larger than the critical angle θ_C. Based on the working theory for the DMD chip, the novel prism design is discussed in terms of angular space and spatial space.

A. Angular Space Condition

The first TIR surface is utilized to avoid interference between the illumination ray path and the image ray path in the projection system [15]. In Fig. 1, the black line represents the illumination ray path and the blue line represents the image ray path. According to the working theory, the illumination rays strike the first TIR surface at an angle larger than the θ_C, so the rays will be reflected into the DMD chip by the TIR condition. After the rays strike the DMD chip they are reflected as image rays in the on state. The image rays strike the second TIR surface at an angle smaller than the θ_C and so just pass through the second TIR surface without being reflected. As can be seen in Fig. 1, at the on state

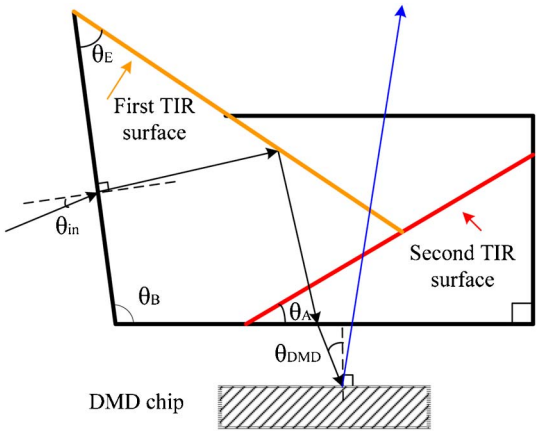

Fig. 1. Schematic diagram of the novel prism, consisting of three transparent prisms at the on state of the DMD chip.

of the DMD chip, the θ_E should be large enough that the rays can strike the first TIR surface at an angle larger than the θ_C. Thus, they can be directed to the DMD chip. Equation (1) shows the limitation of θ_E. Here n_p means index of the prism and F indicates the f-number of the illumination system:

$$\theta_E > \sin^{-1}\frac{1}{n_p} + \sin^{-1}\left\{\frac{1}{n_p}\sin\left[\theta_{in} + \sin^{-1}\left(\frac{1}{2F}\right)\right]\right\}. \quad (1)$$

However, as the θ_E become larger, the size of the prism also gets larger. To keep the prism at a proper size, the θ_E should be controlled to a proper degree.

In the DLP projection system, the image light path can be divided into three states, the on state, flat state, and off state, depending on the DMD chip condition. The flat state is the main type of uncontrolled light leading to scattering issues [8]. The second TIR surface was designed for on-state light and flat-state light. After light is reflected from the DMD chip, the on-state light simply passes through the second TIR surface without TIR condition. This is the first limitation. On the other hand, the DMD chip being at flat state, the flat-state light is reflected away from the projection lens at the second TIR surface with TIR condition. This is the second limitation. There are two limitations in the design of the θ_A. For the illumination ray path with the first limitation, we want the illumination rays to just pass the second TIR surface without being reflected. The first limitation of θ_A is shown in Eq. (2):

$$\theta_A < \sin^{-1}\frac{1}{n_p} + \sin^{-1}\frac{\sin\left[\theta_{\mathrm{DMD}} - \sin^{-1}\left(\frac{1}{2F}\right)\right]}{n_p}. \quad (2)$$

Along the image ray path with the second limitation, the on-state light should pass through the second TIR surface without being reflected while the flat-state light should be reflected at the second TIR surface due to the TIR condition. To achieve this goal, the proper θ_A should be designed. Without considering aberrations, there is no overlap between the on-state light and the flat-state light in the angle space, so there exists a limited θ_A with which to achieve the goal. The second limitation of θ_A is shown in Eq. (3):

$$\theta_A > \sin^{-1}\left(\frac{1}{n_p}\right) - \sin^{-1}\frac{\sin\left[\theta_{\mathrm{DMD}} - \sin^{-1}\left(\frac{1}{2F}\right)\right]}{n_p}. \quad (3)$$

The θ_{DMD} is determined by θ_B and θ_E. The relationship between θ_B, θ_E, and θ_{DMD} is shown in Eq. (4) [15]:

$$\theta_B = 180^\circ + \sin^{-1}\left(\frac{1}{n_p}\sin\theta_{in}\right) - 2\theta_E + \sin^{-1}\left(\frac{1}{n_p}\sin\theta_{\mathrm{DMD}}\right). \quad (4)$$

In the DLP projection system, the tilt angle of the micromirrors on the DMD chips is related to the f-number of the illumination system. The equations mentioned above can still work correctly with different tilt angles of the micromirrors on the DMD chips [6].

B. Spatial Space Condition

In spatial space, the position of the second TIR surface, which affects the ray tracing sequence, is limited. If the light does not follow the ray tracing sequence as in the theoretical design, the total flux of uncontrolled light will increase and there will be a decrease in the projector system's contrast ratio. Figure 2 shows the theoretical ray tracing sequence when the DMD chip is in the flat state. The upward marginal ray represents the top edge of the illumination light cone, and the downward marginal ray represents the bottom edge. The black lines represent the illumination rays, and the blue lines represent the image rays. The illumination rays are directed first to the DMD chip. After being reflected by the DMD chip in the flat state, the flat-state light is directed away from the projection lens by the second TIR surface. The positioning of the second TIR surface ensures the correct ray tracing sequence. If the position of the second TIR surface overlaps limitation point 1, the downward marginal rays will not be directed to the DMD chip. In addition, if the position of the second TIR surface overlaps limitation point 2, the upward marginal rays will not be directed away from the projection lens.

For ease of description, a coordinate axis is shown in Fig. 2. The origin is located at the middle of the entrance surface of the novel prism. Equation (5) is used to calculate the position of limitation point 1 (a,b). Here d_1 is the distance that the chief illumination ray is traced in the novel prism; d_2 is the distance between the DMD chip and the novel prism; t is the transversal distance of the DMD chip; and k is the difference between the clear aperture and the finish dimension of the novel prism. The up and down marginal rays follow the working principles of the

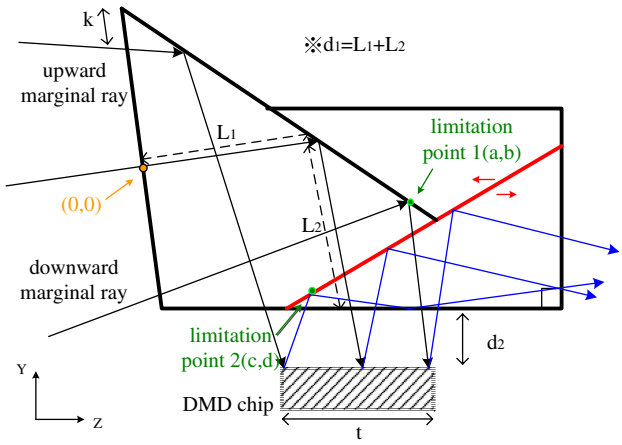

Fig. 2. Ray tracing sequence when DMD chip is in the flat state and the limitation points.

novel prism, and limitation point 1 (a,b) is found as follows:

$$a = \frac{t + 2d_2 \tan\left(\sin^{-1}\frac{1}{2F}\right) + 2d_1 \tan\left(\sin^{-1}\frac{1}{2F\times n_p}\right)}{\tan\left(\theta_B - 90° + \sin^{-1}\frac{1}{2F\times n_p}\right) + \tan(180° - \theta_B - \theta_E)}, \tag{5-1}$$

$$b = -\tan(180° - \theta_B - \theta_E) \times \frac{t + 2d_2 \tan\left(\sin^{-1}\frac{1}{2F}\right) + 2d_1 \tan\left(\sin^{-1}\frac{1}{2F\times n_p}\right) + k}{\tan\left(\theta_B - 90° + \sin^{-1}\frac{1}{2F\times n_p}\right) + \tan(180° - \theta_B - \theta_E)} + \frac{t}{2} + d_2 \tan\left(\sin^{-1}\frac{1}{2F}\right) + d_1 \tan\left(\sin^{-1}\frac{1}{2F\times n_p}\right). \tag{5-2}$$

Equation (6) shows the position of limitation point 2 at (c,d):

$$c = d_1 - \left[\frac{t}{2} + d_2 \tan\left(\sin^{-1}\frac{1}{2F}\right) + d_1 \tan\left(\sin^{-1}\frac{1}{2F\times n_p}\right) + k\right], \tag{6-1}$$

$$d = -\left[\frac{t}{2} + d_2 \tan\left(\sin^{-1}\frac{1}{2F}\right) + d_1 \tan\left(\sin^{-1}\frac{1}{2F\times n_p}\right) + k\right]. \tag{6-2}$$

With Eqs. (1), (2), (3), (4), (5), and (6), the model of the novel prism can be built. Figure 3 shows the ray paths for the on state, flat state, and off state with the second TIR surface at the proper position. The on-state light enters the projection lens without being reflected by the second TIR surface, as shown in Fig. 3(a). The flat-state and the off-state light are directed away from the projection lens when the light encounters the second TIR surface, shown in Figs. 3(b) and 3(c). The flat-state and off-state light are reflected to a light absorber, so the unwanted housing can be avoided.

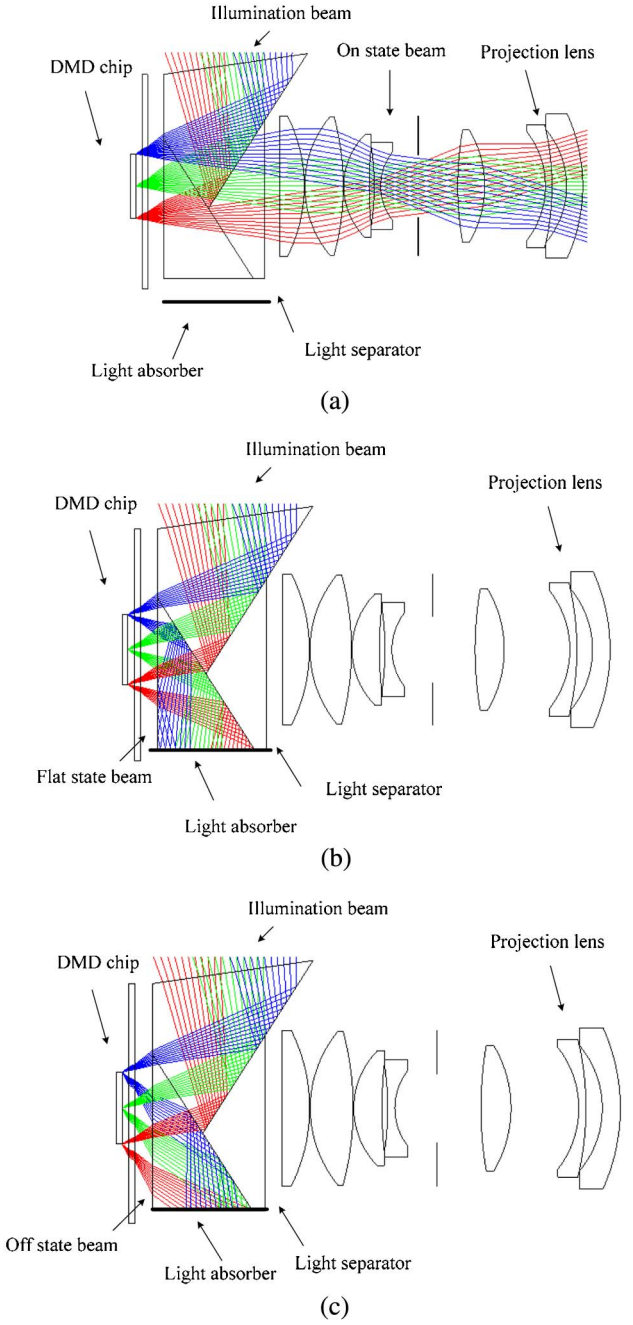

Fig. 3. Arrangement of the DMD chip, the novel prism, and the projection lens: (a) on-state light is directed into the projection lens, (b) flat-state light and (c) off-state light are reflected away from the projection lens.

3. Optical Simulation

A. Projection System with Novel Prism

An LED DLP projector incorporating this novel prism is illustrated in Fig. 4. The DLP projection system was constructed by the LightTools software [17]. It consisted of three subsystems: the illumination system, the relay system, and the projection system. The RGB LED was used as this system's light source. The light is first collected by the illumination system, then passes through the relay system and strikes the DMD chip. The micromirrors on the DMD chip steer the image rays into or away from the projection lens to let the pixels on the screen become bright or dark. In this simulation, the f-number of the illumination system was 2.4 and the θ_{DMD} was set to 26° [8]. The size of the DMD chip was 0.55 in. (13.97 mm) and the tilt angle of the DMD chip was ±12°. The f-number of the projection lens was 2.0 for high efficiency.

B. Analysis of the Contrast Ratio for the Novel Prism

There are two common definitions for projector contrast: The full-on/full-off (FO:FO) contrast ratio [18] and the American National Standards Institute

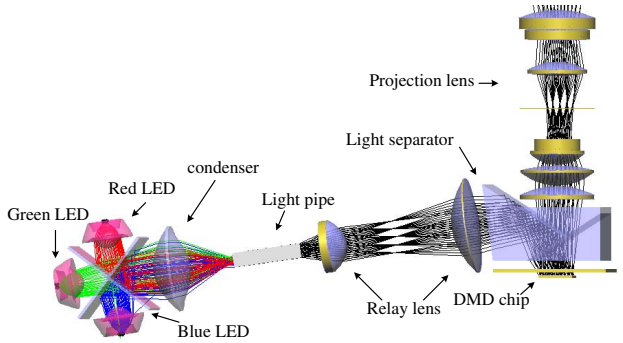

Fig. 4. Schematic diagram of the DLP projector with novel prism.

(ANSI) contrast ratio [19]. The FO:FO contrast ratio is defined as in Eq. (7):

$$\text{FO:FO contrast ratio} = \frac{L(\text{white})}{L(\text{black})}, \tag{7}$$

where L(White) is the illuminance at the center of the screen when the projector is presenting a 100% white level; L(black) is the illuminance at the center of the screen when the projector is presenting a 100% black level. The ANSI contrast ratio determines the proportion of white and black levels when a 4×4 checkerboard pattern is projected on the screen [19]. The definition of imaging system efficiency is the photometric flux on the screen divided by the photometric flux in the receiver between the novel prism and cover glass.

The relationship of the imaging system efficiency and FO:FO contrast ratio versus θ_A is shown in Fig. 5. As the θ_A increases, more flat-state light is reflected by the second TIR surface, so the FO:FO contrast ratio becomes larger. Moreover, as the θ_A increases, less on-state light is collected by the projection lens pupil, so the imaging system efficiency decreases gradually. There is a trade-off between the FO:FO contrast ratio and the imaging system efficiency. In Fig. 5, we can see the balance between the FO:FO contrast ratio and imaging system efficiency. However, the FO:FO contrast ratio is more stable when the θ_A increased to 32.7°. For fabrication tolerances, we set $\theta_A = 32.7°$ as our design [20]. The imaging system efficiency is about 79.8%, and the FO:FO contrast ratio can be enhanced to 46347:1.

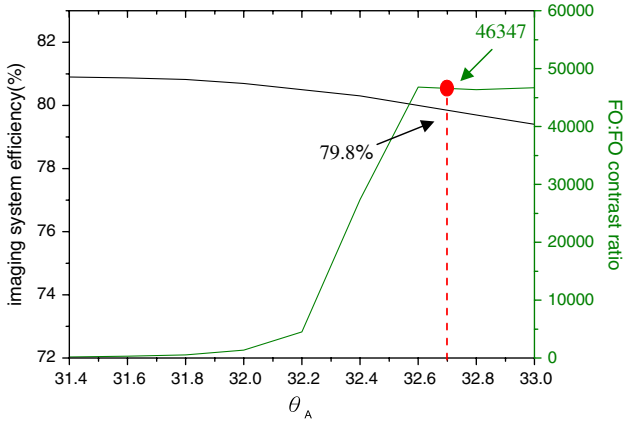

Fig. 5. FO:FO contrast ratio and imaging system efficiency versus θ_A using the novel prism.

In Fig. 5, the speed of increase of the FO:FO contrast ratio slows down after θ_A exceeds 32.6°. As the θ_A increases after this point, all the flat-state light is reflected by the second TIR surface. The remaining uncontrolled light is generated by the Fresnel reflection and cannot be blocked with increasing θ_A.

The simulation result, $\theta_A = 32.7°$, is larger than the result obtained with Eq. (3), $\theta_A = 32°$. To find the proper value of θ_A, there should exist a 0.7° margin in the balance between the FO:FO contrast ratio, imaging system efficiency, and fabrication tolerances.

C. Comparison to the Traditional Prism with an Asymmetric Stop

The asymmetric stop method is popularly used for contrast enhancement in the traditional DLP projector [8,9,11,21]. In this simulation, the contrast enhancement for a conventional prism with an asymmetric stop is realized without changing other elements. For convenience, a knife edge is used as the projection lens stop when simulating the asymmetric stop. Figure 6 shows the relationship between the projection lens stop and the asymmetric stop. The asymmetric stop is aligned normal to the rotation trajectory of the micromirrors on the DMD chip. Here $\beta = 0$ indicates when the asymmetric stop is located at the edge of the projection lens stop. The asymmetric stop does not block any light passing through the projection lens. As β increases, the asymmetric stop moves closer to the center of the projection lens stop. The relationship between the imaging system efficiency and the FO:FO contrast ratio versus asymmetric stop position is shown in Fig. 7.

From Fig. 7, it can be seen that when the asymmetric stop position β increases to 1 mm, there is a balance between the FO:FO contrast ratio and imaging system efficiency. Moreover, the imaging system efficiency is about 80.9%, and the FO:FO contrast ratio is 921:1.

The ANSI contrast is also an important consideration for image quality. We compare the ANSI

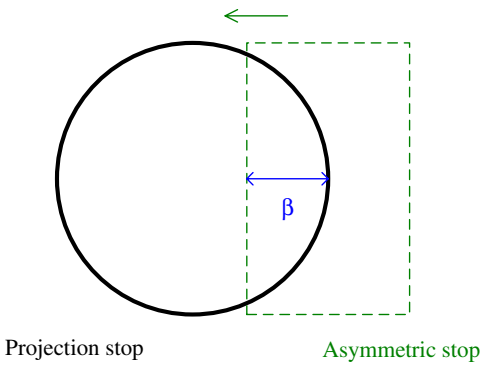

Fig. 6. Schematic diagram of projection lens stop with asymmetric stop.

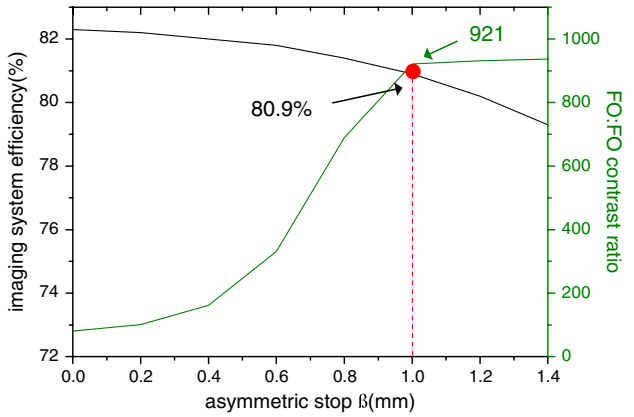

Fig. 7. FO:FO contrast ratio and imaging system efficiency versus asymmetric stop position in a conventional prism.

contrast ratio performance obtained using two different processes but the same optical engine. The ANSI contrast ratio for the novel prism and asymmetric stop are shown in Fig. 8. The results indicate greater enhancement of the inherent ANSI contrast ratio with the novel prism than with the conventional prism with an asymmetric stop. The ANSI contrast ratio increases from 231:1 to 296:1 for the novel prism when θ_A increases from 31.4° to 33.0°. However, the contrast ratio can be increased from 146:1 to 181:1 by moving the asymmetric stop from 0.0 to 1.4 mm.

Finally, the contrast ratio, ANSI contrast ratio, and imaging system efficiency obtained with the two prisms are compared in Table 1. Under a contrast enhancement process with the same imaging system efficiency, the FO:FO contrast ratio obtained with the novel prism is higher than the one obtained with the conventional prism. Moreover, the ANSI contrast obtained with the novel prism is also higher than the ANSI contrast obtained with the conventional prism. The simulation results show the

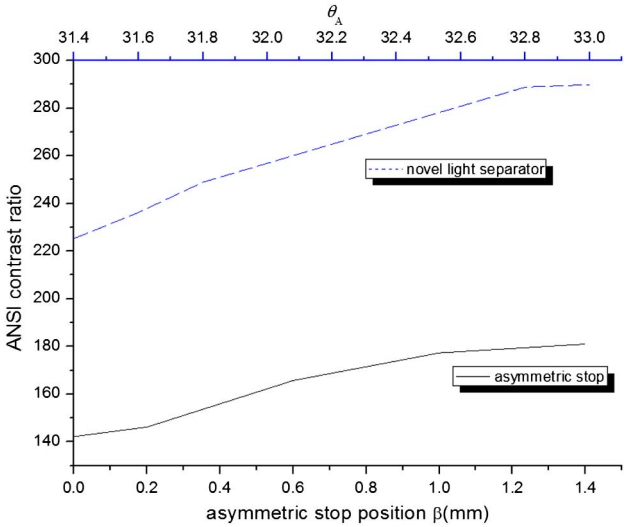

Fig. 8. Comparison of the ANSI contrast ratios obtained with the novel prism and asymmetric stop.

Table 1. Results of the Simulations

	Asymmetric Stop with Convention Prism ($\beta = 1$ mm)	Novel Prism ($\theta_A = 32.7°$)
FO:FO contrast ratio	921:1	46347:1
ANSI contrast ratio	177:1	295:1
Imaging system efficiency	80.9%	79.8%

superiority of the novel prism. Its design parameters are shown in Table 2. The critical point is the intersection point between the second TIR surface and the bottom surface of the novel prism. An example of the novel prism is shown in Fig. 9. For the testing results of the system with this novel prism, the FO:FO contrast ratio and ANSI contrast ratio are 2050:1 and 206:1, respectively.

4. Ghost Ray Analysis

According to the above analysis, the contrast ratios are higher for the novel prism than the conventional prism with an asymmetric stop. The higher contrast ratios indicate that the novel prism should have better ghost ray control performance. To find the reason

Table 2. Parameters of the Novel Prism

θ_{in} (deg)	0
f-number	2.4
t (mm)	13.97
k (mm)	1.20
d_1 (mm)	31.90
d_2 (mm)	5.14
θ_B (deg)	98.2
θ_E (deg)	49.3
θ_A (deg)	32.7
Limitation point 1 (a,b)	(27.01,–4.70)
Limitation point 2 (c,d)	(18.19,–13.70)
Critical point	(14.00,–13.70)

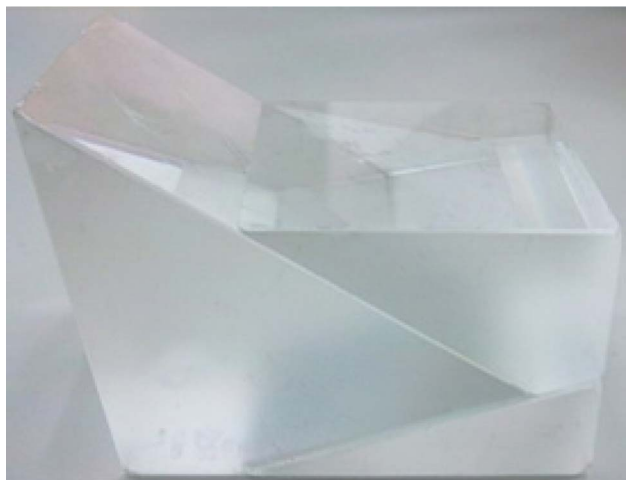

Fig. 9. Example of the novel prism.

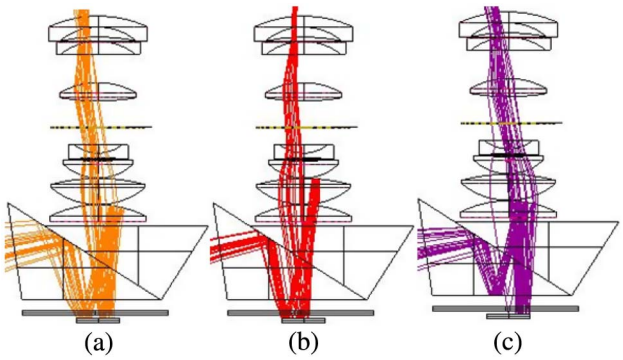

Fig. 10. Three main ghost ray paths in model 1: (a) path 1, (b) path 2, and (c) path 3.

why the novel prism is able to achieve a greater reduction of ghost rays, we carry out a ghost ray analysis using the two contrast ratio enhancement processes and the ray path function for a flat-state DMD chip with the LightTools software. Model 1 is the projection system with the conventional prism and the asymmetric stop. Figure 10 shows the three main ghost ray paths in model 1: paths 1, 2, and 3. Paths 1 and 2 are caused by Fresnel reflection when the flat-state light passes through the projection lens. The DMD chip is in the flat state, and Fresnel reflection occurs in the rear part of the telecentric projection lens. In model 1, ghost ray path 1 produces about 4.82 lm (63.5%) and ghost ray path 2 produces about 0.53 lm (7%). These two paths are the main component of the ghost ray in model 1. Ghost ray path 3 first strikes the bottom surface of the conventional prism and then passes through the telecentric projection lens. Ghost ray path 3 is caused by the bottom surface of the conventional prism and the rear part of the telecentric lens. In model 1 this ghost ray path produces about 0.12 lm (1.6%) for a total in model 1 of 7.6 lm. Table 3 shows the ghost ray analysis data used for model 1. According to the data, there are three ghost ray paths relative to the DMD chip and the rear part of the telecentric projection lens. The only way to eliminate the ghost ray before it hits the rear part of the telecentric projection lens is to use the novel prism to change the path and the ghost light energy flux.

Model 2 is the projection system with a novel prism. Figure 11 shows the two main ghost ray paths in model 2, path 1 and path 2. Paths 1 and 2 in model 2 are just like path 3 in model 1. The ghost ray is caused by the Fresnel reflection at the bottom surface of the novel prism and the rear part of the telecentric projection lens. In model 2, ghost ray path 1 produces about 0.107 lm (76.4%) and ghost ray path 2 produces about 0.02 lm (19.4%) for a total in model 2 of 0.141 lm. Table 4 shows the ghost ray analysis data used in model 2.

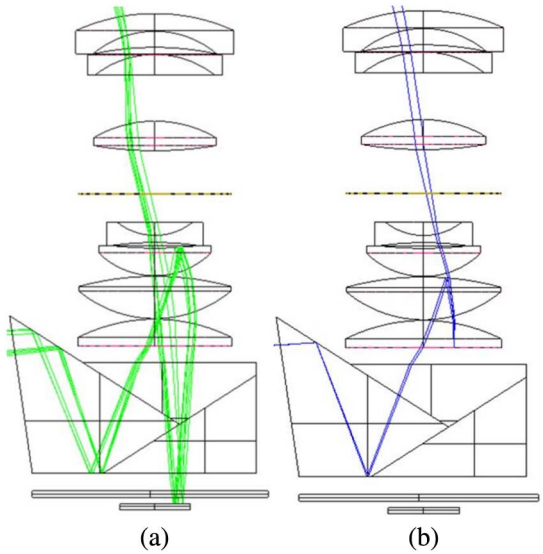

Fig. 11. Two main ghost ray paths in model 2: (a) path 1 and (b) path 2.

Comparison of the results of ghost ray analysis between the two models shows that ghost ray path 1 and ghost ray path 2 in model 1 can be eliminated by applying a second TIR surface, as is done with the novel prism in model 2. The two ghost ray paths were caused by Fresnel reflection when the flat-state light passed through the projection lens. However, in the novel prism, the flat-state light is directed away from the projection lens. Since the flat-state light does not enter the projection lens, model 1's ghost ray paths 1 and 2 do not happen in model 2. The two main ghost ray paths that appear in model 1 can be successfully eliminated by using the novel prism so that better contrast ratio enhancement can be easily achieved in model 2. However, model 1's path 3 still happened in model 2, which means that this ghost ray path cannot be totally eliminated by replacing the conventional prism and asymmetrical stop with the novel prism. However, this disadvantage can be improved by the application of an antireflection coating to the bottom surface of the novel prism and at the rear part of the telecentric projection lens. In a word, the bottom surface of the two prisms is critical for the contrast ratio.

Table 3. Ghost Ray Analysis Data Used in the Conventional Prism Projection System

	Luminous Flux (lm)	Percentage (%)
Ghost ray path 1	4.82	63.5
Ghost ray path 2	0.53	7
Ghost ray path 3	0.12	1.6
Total ghost ray	7.6	100

Table 4. Ghost Ray Analysis Data Used in the Projection System with a Novel Prism

	Luminous Flux (lm)	Percentage (%)
Ghost ray path 1	0.107	76.4
Ghost ray path 2	0.027	19.4
Total ghost ray	0.141	100

5. Conclusion

In this paper, a novel prism with the ability to enhance the contrast ratio while maintaining the optical efficiency of a DLP projection system is proposed. Utilizing the flat-state DMD chip, this novel prism has the main function to direct uncontrolled light away from the projection lens. This novel prism design can enhance the contrast ratio over that obtained with the asymmetric stop projection lens. Compared with the conventional method, the FO: FO contrast ratio can be improved from 921:1 to 46347:1 and the ANSI contrast ratio can be improved from 177:1 to 295:1. Moreover, the imaging system efficiency remains at 79.8%. Ghost ray analysis is carried out. The ghost ray component can be realized. The difference between the novel prism and asymmetric stop can be easily understood. We can see that the bottom surface of the separator is the main reason for the ghost rays. With the advantage of high contrast ratio, the projector can project a more vivid image and the image quality can be greatly improved.

This study was supported in part by the National Science Council, project numbers NSC101-2220-E-009-022, NSC102-2220-E-009-006, and NSC101-2622-E-009-010-CC3, and in part by the Aim for the Top University Plan of the National Chiao Tung University and the Ministry of Education, Taiwan. The optical simulation LightTools software was supported by CYBERNET SYSTEMS TAIWAN under the Synopsys education license agreement.

References

1. X. Zhao, Z. L. Fang, J. C. Cui, X. Zhang, and G.-G. Mu, "Illumination system using LED sources for pocket-size projectors," Appl. Opt. **46**, 522–526 (2007).
2. J. W. Pan and S. H. Lin, "Achromatic design in the illumination system for a mini projector with LED light source," Opt. Express **19**, 15750–15759 (2011).
3. S. P. Marks, "Projector phones: cool app or visual pollution," New Scientist **201**(2697), 18–19 (2009).
4. S. C. Shin, Y. Jung, T. J. Ahn, S. S. Jeong, S. G. Lee, and K. Y. Choi, "The compact systems design based on DMD and the straight line 2-channel LED for a mobile embedded pico projector," J. Display Technol. **8**, 219–224 (2012).
5. L. J. Hornbeck, "Digital light processing for high-brightness, high-resolution applications," Proc. SPIE **3013**, 27–40 (1997).
6. Texas Instruments (TI), "DLP discovery optics 101 application note," http://focus.ti.com/lit/an/dlpa022/dlpa022.pdf.
7. Texas Instruments Incorporated, "Introduction to Digital Micro Mirror Device (DMD) technology," Appl. Rep. DLPA008, 2008.
8. J. W. Pan, C. M. Wang, W. S. Sun, and J. Y. Chang, "Portable Digital Micromirror Device projector using a novel prim," Appl. Opt. **46**, 5097–5102 (2007).
9. Y. Meuret and P. De Visschere, "Contrast-improving methods for Digital Micromirror Device projectors," Opt. Eng. **42**, 840–845 (2003).
10. P. J. Janssen and J. A. Shimizu, "High contrast illumination system for video projector," U.S. Patent 5,442,414 (Aug. 15, 1995).
11. G. P. Pinho, "Optics of digital cinema," Proc. SPIE **5002**, 123–131 (2003).
12. W. J. Smith, *Modern Optical Engineering*, 4th ed. (McGraw-Hill, 2008), pp. 185–186.
13. J. W. Pan, S.-H. Tu, C.-M. Wang, and J.-Y. Chang, "High efficiency pocket-size projector with a compact projection lens and a light emitting diode-based light source system," Appl. Opt. **47**, 3406–3414 (2008).
14. Y. C. Fang, W. T. Lin, and H. L. Tsai, "High-definition DLP zoom projector lens design with TIR prism for high-definition television (HDTV)," Proc. SPIE **6342**, 63420Z (2006).
15. J. W. Bowron and R. P. Jonas, "Off-axis illumination design for DMD systems," Proc. SPIE **5186**, 72–82 (2003).
16. M. Yamanaka and M. Nishio, "Air gap prism and method for producing same," U.S. Patent 5,900,984 (May 4, 1999).
17. Optical Research Associates (ORA). http://optics.synopsys.com/index.html.
18. E. H. Stupp and M. S. Brennesholtz, "Characteristics and characterization," in *Projection Displays*, A. C. Lowe, ed. (Wiley, 1999), Chap. 13, pp. 289–319.
19. American National Standards Institute (ANSI), "American National Standard for Audiovisual Systems-Electronic Projection-Fixed Resolution Projectors," ANSI/NAPM IT7.228-1997, 1997.
20. W. J. Smith, *Modern Optical Engineering* (McGraw-Hill, 2008), pp. 619–621.
21. M. Inamoto, "Asymmetric aperture diaphragm placing structure for projection lens and projection type image display apparatus using the same," U.S. Patent 6,942,349 (13 September, 2005).